DOI: 10.1002/adma.200801224

Highly Efficient Fluorescence of NdF_3/SiO_2 Core/Shell Nanoparticles and the Applications for *in vivo* NIR Detection**

By *Xue-Feng Yu, Liang-Dong Chen, Min Li, Meng-Yin Xie, Li Zhou, Yan Li,* and *Qu-Quan Wang**

The use of near-infrared (NIR) fluorescence is a promising approach for biomedical imaging and detection.[1–6] Such applications with well performances require: (i) the excitation and emission are within 700–1100 nm (the so-called ''NIR optical window'') to provide deeper tissue penetration of photons with reduced photodamage effects,[7] and (ii) a large frequency shift between the emission and excitation to provide an efficient signal-to-noise (S/N) ratio.[3]

Based on these considerations, NIR semiconductor quantum dots (QDs), with brighter fluorescence and larger Stokes shift than organic dyes, have been discussed intensely.[3–5,8] However, they are still controversial because of their inherent toxicity and chemical instability.[9,10] Recently, nanosized materials based on rare-earth (RE) ions (such as Nd^{3+}, Er^{3+}, Ho^{3+}, and Pr^{3+}) have been proposed to be a promising new class of biological NIR probes. Such materials are attractive due to their unique optical and chemical features, such as characteristic sharp fluorescence, long fluorescence lifetime (μs to ms range), good photostability and low toxicity.[11]

In recent years, strategies have been developed to increase the optical capabilities of NIR RE nanoparticles (NPs) via suppressing surface quenching and concentration quenching, which are two main energy-loss effects in RE materials.[12–20] In 2002, van Veggel et al. synthesized NIR RE ions doped LaF_3 NPs which demonstrated excellent optical efficiency in organic solvents,[12] but such NPs were not water-soluble or biocompatible. Subsequently, different methods were designed to prepare water-soluble RE NPs,[14,15] however, the O–H groups on their surfaces noticeably hampered their optical efficiency. To suppress such energy-loss effect caused by the environment, the beneficial influence of passivating inorganic shells (such as undoped $LaPO_4$[16] and LaF_3[17,18]) has impressively been demonstrated in recent literatures.

On the other hand, concentration quenching is another common energy-loss mechanism for fluorescent RE ions, and such phenomenon often occurs at very low ion concentrations (below 1 mol %) in bulk materials.[21] While recent literatures have demonstrated that in some NPs, fluorescent RE ions have unusual thresholds (even near 50 mol %) for the concentration effect.[22–24] This provides new possibility for improving fluorescent RE materials, however, it is still unclear whether there exists some RE NPs which are free from the concentration quenching effect.

In this work, we developed NdF_3/SiO_2 core/shell NPs, which demonstrated highly efficient fluorescence in vivo due to the successful suppressions of these two energy-loss effects as well as satisfying the above-mentioned spectral requirements. Fluoride was chosen because such material has adequate thermal and environmental stability,[25] and large solubility for RE ions without deleterious effects.[26] Particularly, the high ionicity of the RE–fluorine bond leads to a wide bandgap and very low phonon energies. These are especially important for the RE ions emitting in the NIR region.[12,27]

The uniform NdF_3 NPs were synthesized by using a facile route in aqueous solution without any surfactants. Similar method has been used to synthesize traditional Nd^{3+} doped LaF_3 NPs while changing $NdCl_3$ to $LnCl_3$ (Ln = La, Nd).[14] The transmission electron microscopy (TEM) image in Figure 1a shows that the prepared NdF_3 NPs are of nearly spherical shape and have an average diameter of about 30 nm. The thin silica shells were coated over the NdF_3 cores by using the modified Stöber method,[28] and their average thickness is about 4 nm (Fig. 1b). The high-resolution transmission electron microscopy (HRTEM) image (Fig. 1c) and the selected area electron diffraction (SAED) pattern (Fig. 1d) exhibit the hexagonal reciprocal lattice of (237) zone axis of NdF_3 mono-crystalline, and one can readily index the x-ray diffraction (XRD) pattern (Fig. 1e) to the hexagonal phase of NdF_3 with lattice constants $a = 0.7030$ nm and $c = 0.7199$ nm (JCPDS No. 9–416).

[*] Prof. Q.-Q. Wang, Dr. X.-F. Yu, M. Li, M.-Y. Xie, L. Zhou
Department of Physics
Wuhan University, Wuhan, 430072 (P. R. China)
E-mail: qqwang@whu.edu.cn
Prof. Q.-Q. Wang, Dr. X.-F. Yu
Key Laboratory of Acoustic and Photonic Materials and Devices of the Ministry of Education Institution
Wuhan University, Wuhan, 430072 (P. R. China)
Dr. L.-D. Chen, Prof. Y. Li
Department of Oncology, Zhongnan Hospital & Cancer Center of Wuhan University
Wuhan, 430071 (P. R. China)

[**] The authors thank the Natural Science Foundation of China and the National Program on Key Science Research (2006CB921500) for support. X.-F. Yu and L.-D. Chen contributed equally to this work. Supporting Information is available online from Wiley InterScience or from the authors.

ADVANCED MATERIALS

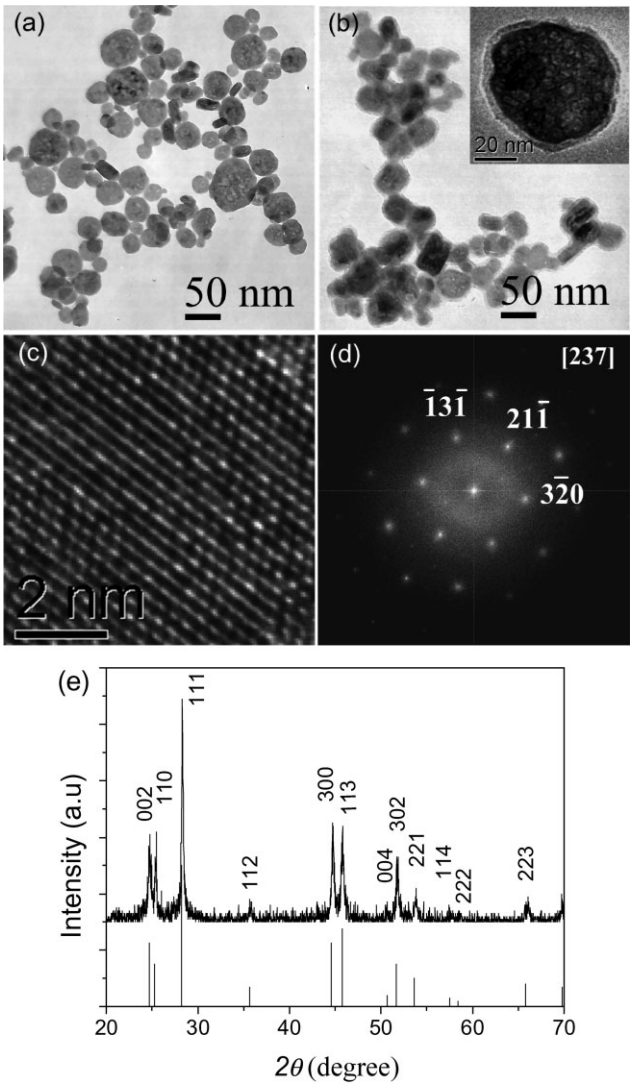

Figure 1. a) and b) TEM images of NdF_3 and NdF_3/SiO_2 NPs. c) and d) HRTEM image and SAED pattern of one particle selected from a. (e) XRD pattern of NdF_3 NPs. The line spectrum corresponds to the literature data of bulk NdF_3 (JCPDS No. 9-416 reference pattern).

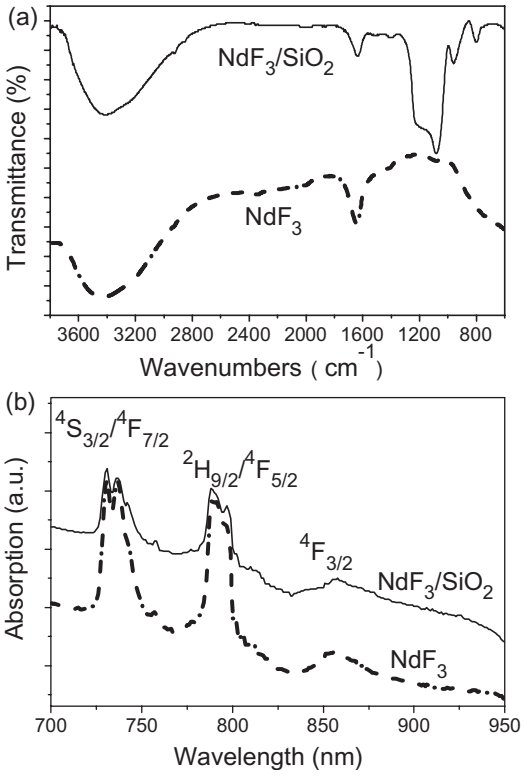

Figure 2. a) FTIR spectra of NdF_3 and NdF_3/SiO_2 NPs. b) Absorption spectra of NdF_3 and NdF_3/SiO_2 NPs in aqueous solution.

Fourier transform infrared (FTIR) was used to investigate the organic residua in the NdF_3 and NdF_3/SiO_2 powders. As the NPs are prepared in water, their surface may be covered by a large number of O–H groups either chemically bonded or physically adsorbed to the surface, as confirmed by the FTIR spectra in Figure 2a. The absorption bands at around 3430 and 1635 cm^{-1} are attributed to O–H stretching and bending vibrations, respectively. In regard to the NdF_3/SiO_2 core/shell NPs, aside from the presence of the characteristic absorption bands of NdF_3, the absorption bands at around 1083 and 799 cm^{-1} are attributed to Si–O–Si asymmetrical and symmetric stretching vibrations, respectively.

The absorption spectra in Figure 2b clearly show the characteristic Nd^{3+} absorption peaks at around 732, 788, and 858 nm in the NIR region.[29] These three absorption bands correspond to the $^4S_{3/2}/^4F_{7/2}$, $^2H_{9/2}/^4F_{5/2}$, and $^4F_{3/2}$ multiplets of Nd^{3+}, respectively.[22]

Figure 3a gives the excitation spectra ($\lambda_{em} = 1056$ nm) of the NdF_3 and 5% Nd^{3+} doped LaF_3 NPs synthesized under the same procedure. Their excitation peaks at around 730, 800, and 870 nm correspond to the above-mentioned absorption bands. As compared to the traditional 5% Nd^{3+} doped LaF_3 NPs, the most efficient excitation peak of the uniform NdF_3 NPs blue-shifts from around 800 to 730 nm. In practical bio-applications, tissue autofluorescence and excitation-scattered light are great obstacles, increasing background noise. So the NdF_3 NPs, providing a frequency separation as large as 4229 cm^{-1}, have the potential to increase the S/N ratio in tissue studies.

On the other hand, the emission spectrum ($\lambda_{ex} = 730$ nm) of the NdF_3 NPs (Fig. 3b) shows typical emissions at around 868 and 1056 nm corresponding to the $^4F_{3/2} \rightarrow {}^4I_{9/2}$ and $^4F_{3/2} \rightarrow {}^4I_{11/2}$ transitions of Nd^{3+}, respectively. Considering both the most efficient excitation (730 nm) and emission (1056 nm) peaks are all within the NIR window, the NdF_3 NPs can provide both deeper penetration of photons from the excitation and greater escape depths for the emission in biological samples.

The spectra in Figure 3b also show that the fluorescence intensity at 1056 nm of the uniform NdF_3 NPs is about 5.1 times that of the 5% Nd^{3+} doped LaF_3 NPs. Further, while increasing

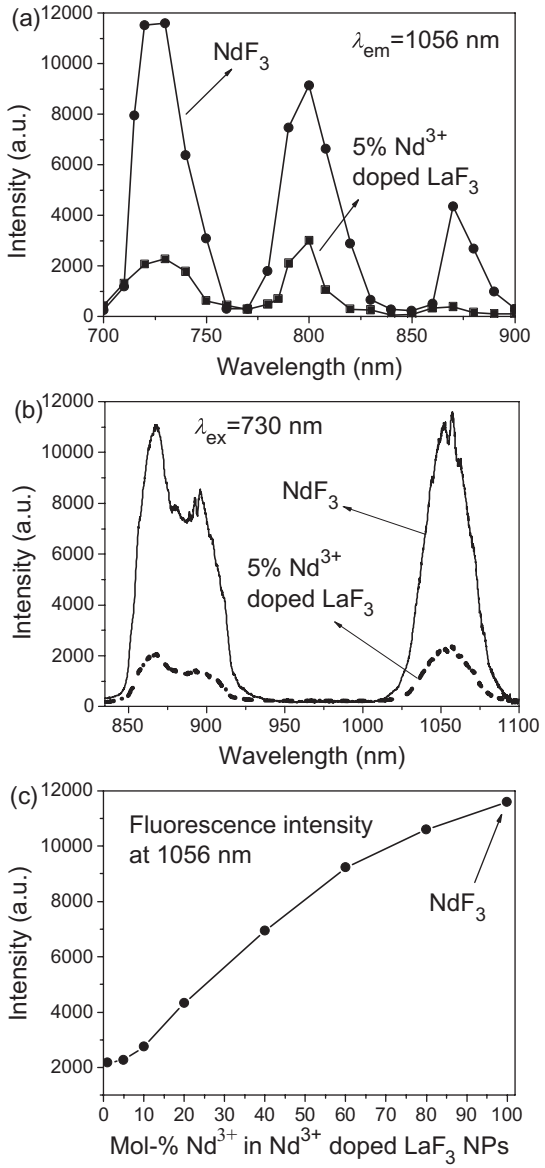

Figure 3. a) and b) Excitation (a, $\lambda_{em} = 1056$ nm) and emission (b, $\lambda_{ex} = 730$ nm) spectra of NdF_3 and 5% Nd^{3+} doped LaF_3 NPs in aqueous solution. (c) Fluorescence intensity at 1056 nm ($\lambda_{ex} = 730$ nm) versus mole percent (x %) of Nd^{3+} in Nd^{3+} doped LaF_3 NPs. The molar concentration of the RE ions (including La^{3+} and Nd^{3+}) in all the above samples is 5.0 mM.

the molar percent (x %) of Nd^{3+} in the Nd^{3+} doped LaF_3 NPs, the fluorescence at 1056 nm increases remarkably and reaches the maximum when x % = 100% (Fig. 3c). The results imply that the concentration quenching effect does not occur in the nanosized Nd^{3+} doped fluorides. Such no concentration quenching phenomenon has been predicted by Zhang et al. and Wei et al.,[30,31] and similar uniform fluorescent RE NPs, such as EuF_3,[32] CeF_3,[33] $NdVO_4$,[34] and Nd_2O_3,[35] have begun to attract much attention very recently. In RE materials, quenching originates in a very efficient energy transfer among the RE ions. Due to the match of their energy levels, the eventual energy transfers from the RE ions to a defect where non-radiative decay occurs.[36] In nanomaterials, such non-radiative energy transfer only occurs within one particle due to the hindrance of the particle boundary,[22,24] so quenching often occurs at much higher ion concentration compared with that in their bulk counterparts. Further, if the defect concentration is low enough in the nanomaterial, due to the physical volumetric constrains of the nanomaterial (10^{-7} smaller than the bulk),[36] there is a reasonable probability that in some particles RE ions in the 'ion chain' will have no neighbor defect, thus only radiative decay occurs. Consequently, those NPs quench at only high ion concentration or do not quench at all.[30,31] Although the mechanism of such phenomenon still needs more detailed investigations (the discussion about the emission quantum efficiency is shown in the Supporting Information), the results here provide new possibilities for improving fluorescent RE materials.

Moreover, to suppress the vibrational quenching caused by the O–H groups on the surfaces of the NdF_3 NPs, silica shells were coated and the core/shell structures were annealed at 300 °C for 3 h to obtain NdF_3/SiO_2 NPs. The O–H groups are reduced by the annealing process, and then the Nd^{3+} ions inside are protected by the annealed silica shells in aqueous solution. The spectra in Figure 4 show that the fluorescence intensity of the NdF_3/SiO_2 NPs is about 1.6 times that of the bare NdF_3 NPs at the same mass concentration in aqueous solution. Similar beneficial influences of passivating inorganic shells[16–18] and thermal treatment[37–39] have been demonstrated in recent literatures. It should be noted that the annealed bare NdF_3 NPs are not water-soluble. Moreover, since the surface chemistry of silica particles is well documented and silica is known to have benign effects in biological systems,[40] the use of a silica coating over RE materials is an attractive alternative for bio-applications. As such, we employed the NdF_3/SiO_2 NPs as probes for the following biological investigations.

For deep tissue imaging, one mouse was injected intramuscularly and intraperitoneally with 100 μL of NdF_3/SiO_2 NPs

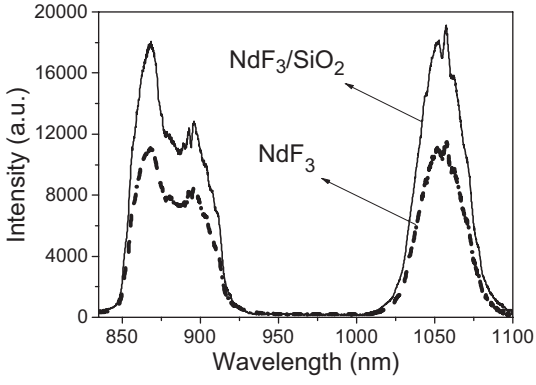

Figure 4. Emission spectra ($\lambda_{ex} = 730$ nm) of NdF_3 and NdF_3/SiO_2 NPs in aqueous solution (1.0 mg mL^{-1}). It should be noted that we can obtain 105 mg NdF_3/SiO_2 NPs from 100 mg NdF_3 NPs.

ADVANCED MATERIALS

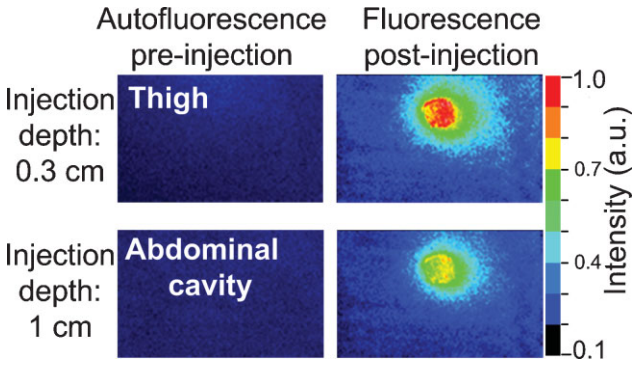

Figure 5. Deep tissue imaging at the thigh and abdominal cavity in one nude mouse, after injected intramuscularly and intraperitoneally with 100 μL of NdF_3/SiO_2 NPs (1.0 μg mL^{-1}), respectively. Left, Autofluorescence images pre-injection. Right, Fluorescence images post-injection. The injection depths of the thigh and abdominal cavity were about 0.3 and 1 cm, respectively.

(1.0 μg mL^{-1}) into the thigh and abdominal cavity, respectively. During *in vivo* experiments, NIR-excitation was with a 730 nm CW laser (100 mW output power) and the field of view for imaging and detection was 1 cm in diameter. A band-pass filter (1050/10 nm) was used for spectral imaging and the images had identical exposure time (1 min) and normalization. The images in Figure 5 show that the particle signals from the deep tissues of the thigh and abdominal cavity are both clearly distinguished from the tissue autofluorescence. Under local injection, the abdominal cavity is the deepest area (about 1 cm to the skin surface) that one can choose in a living mouse. So the results here indicate that the NdF_3/SiO_2 NPs are efficient enough for deep tissue detection in small animals. We note that the quantity here (100 μL at 1.0 μg mL^{-1}) is much less than the amount of up-converted $NaYF_4$:Yb,Er NPs (100 μL at 4.4 mg mL^{-1}) used in a recent work involving a similar mouse model.[41]

Another mouse was injected with 200 μL of NdF_3/SiO_2 NPs (5.0 μg mL^{-1}) into the tail vein. During the first 30 min post-injection, the emission from one earlobe vessel was recorded repeatedly every 10 s and the exposure time for each spectrum was 100 ms. The typical spectra in Figure 6a show both the clear particle signal and the faint background noise from the tissue autofluorescence. The very high S/N ratio at 1056 nm (over 15 at least) was attributed to the highly efficient fluorescence from the NdF_3/SiO_2 NPs and large frequency separation to the excitation at 730 nm. Further, considering the exposure time for each spectrum was very short, the variation of the particle signal was sensitive enough to indicate the particle flow in body fluids (shown in Fig. 6b). The spectrum in the inset of Figure 6b indicates that NdF_3/SiO_2 NPs demonstrate excellent photostability in mouse whole blood in vitro. In contrast, the particle fluorescence from the earlobe vessel changed continuously during the monitoring period, indicating the NPs did not aggregate or obstruct in body fluids. The fluorescent variation show that the signal intensity

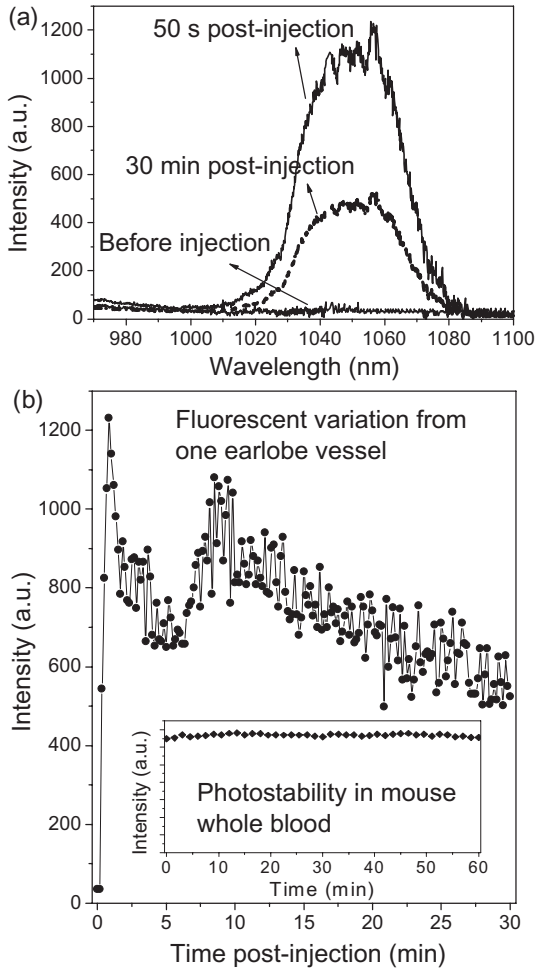

Figure 6. a) Fluorescence spectra from one earlobe vessel of a nude mouse before and after injected with 200 μL of NdF_3/SiO_2 NPs (5.0 μg mL^{-1}) into the tail vein. b) Fluorescence monitoring from the earlobe vessel during the first 30 min post-injection; inset shows the photostability of NdF_3/SiO_2 NPs in the mouse whole blood (1.0 mg mL^{-1}) *in intro* under a 100 mW 730 nm CW laser excitation.

fluctuated within the first 9 min post-injection due to the inhomogeneous particle flow during the initial systemic circulation, and the following weakened signal intensity was caused by the non-specific particle uptake by the organs. These data suggest that such material can find use in pharmacokinetics studies while coupling with some plasma drugs. After in vivo experiments, no toxicity or other physiological complications were observed for the animals after at least 24 h of particle injection (the detailed toxicity test is shown in the Supporting Information).

In conclusion, we open the door to using NIR RE NPs as probes for in tissue studies. The developed material is attractive due to its unique excitation and emission spectral characteristics, excellent photostability, low toxicity and highly efficient fluorescence in living tissues. To the best of our knowledge, this represents the first report of in vivo NIR detection by using RE NPs.

Experimental

Synthesis of NdF_3 Nanoparticles: All chemicals were purchased from Sigma–Aldrich and used without further purification. A sodium fluoride (NaF) solution (10 mL, 0.2 M) was added dropwise into a neodymium chloride hexahydrate ($NdCl_3 \cdot 6H_2O$) solution (40 mL, 0.04 M) and the mixture was subsequently heated to 75 °C for 2 h under stirring. The resulting suspension was centrifuged (10 min, 10 000 *g*) and washed with distilled water 3 times. The precipitates were then dried under vacuum, and a lavender powder of NdF_3 was obtained.

Synthesis of NdF_3/SiO_2 Nanoparticles: 100 mg of NdF_3 NPs dissolved in distilled water (5.1 mL) were added to an ethanol (14.0 mL) and NH_4OH (0.3 mL) mixture. Immediately, 0.1 mL tetraethylorthosilicate (TEOS) was added dropwise and the mixture was stirred for 60 min. The resulting suspension was centrifuged (10 min, 10 000 *g*) and washed with ethanol 3 times. The precipitates were dried and annealed at 300 °C for 3 h in air. At last, 105 mg of NdF_3/SiO_2 NPs were obtained.

Characterization: The TEM and HRTEM images were measured with a JEOL 2010 HT and JEOL 2010 FET transmission electron microscope (operated at 200 kV), respectively. XRD analyses were performed on a Bruker D8-advance X-ray diffractometer with Cu kα irradiation ($\lambda = 1.5406$ Å). The absorption spectra were measured using a Varian Cary 5000 UV/vis/NIR spectrophotometer. FTIR spectra were recorded on an AVATAR-360 spectrometer. A small amount of powder samples were mixed with KBr and then pressed to make a thin pellet for FTIR studies.

Optical Measurements: The excitation source for the fluorescence spectra and images was a Ti: Sapphire CW laser (Mira 900, Coherent) with tunable wavelength in the range 700–1000 nm. A long-wavelength pass filter and a tunable neutral density filter were used to filter the short wavelength noise from the laser and adjust the intensity of the excitation, respectively. The fluorescence spectra were recorded by a spectrometer (Spectrapro 2500i, Acton) with liquid nitrogen cooled CCD (SPEC-10: 100B, Princeton) and corrected with the spectroscopy quantum efficiency curves.

In vivo Studies: Using protocols approved by the Institutional Animal Care and Use Committee of Wuhan University, 6-week-old nude mice were placed under anesthesia by injection of 3% Nembutal at a dosage of 45 mg kg^{-1} for in vivo studies. The NdF_3/SiO_2 NPs were sterile-filtered and stored in PBS solution (pH 7.4). For deep tissue imaging, one mouse was injected intramuscularly and intraperitoneally with 100 μL of NdF_3/SiO_2 NPs (1.0 μg mL^{-1}) into the thigh and abdominal cavity, respectively. Another mouse was injected with 200 μL of NdF_3/SiO_2 NPs (5.0 μg mL^{-1}) into the tail vein for monitoring the particle fluorescence from one earlobe vessel within the first 30 min post-injection. NIR-excitation was with a 730 nm CW laser (100 mW output power) and the field of view for imaging and detection was 1 cm in diameter. The above-mentioned CCD and a band-pass emission filter 1050/10 nm (center wavelength = 1050 nm, half width = 10 nm, Andover corporation) were used for spectral imaging. Two collected filters (both the focus lengths of the lens are 100 mm) were used before the CCD to obtain 3 times reduced fluorescence images. The exposure time for each image was 1 min and the collected images were analyzed by the WinSpec/32 software.

Received: May 3, 2008
Published online:

[1] R. Weissleder, C. H. Tung, U. Mahmood, A. Bogdanov, Jr, *Nat. Biotechnol.* **1999**, *17*, 375.
[2] M. Hintersteiner, A. Enz, P. Frey, A. L. Jaton, W. Kinzy, R. Kneuer, U. Neumann, M. Rudin, M. Staufenbiel, M. Stoeckli, K. H. Wiederhold, H. U. Gremlich, *Nat. Biotechnol.* **2005**, *23*, 577.
[3] S. Kim, Y. T. Lim, E. G. Soltesz, A. M. Grand, J. Lee, A. Nakayama, J. A. Parker, T. Mihaljevic, R. G. Laurence, D. M. Dor, L. H. Cohn, M. G. Bawendi, J. V. Frangioni, *Nat. Biotechnol.* **2004**, *22*, 93.
[4] W. Cai, D. W. Shin, K. Chen, O. Gheysens, Q. Cao, S. X. Wang, S. S. Gambhir, X. Chen, *Nano Lett.* **2006**, *6*, 669.
[5] P. Diagaradjane, J. M. Orenstein-Cardona, N. E. Colón-Casasnovas, A. Deorukhkar, S. Shentu, N. Kuno, D. L. Schwartz, J. G. Gelovani, S. Krishnan, *Clin. Cancer Res.* **2008**, *14*, 731.
[6] Q. le Masne de Chermont, C. Chanéac, J. Seguin, F. Pellé, S. Maîtrejean, J. P. Jolivet, D. Gourier, M. Bessodes, D. Scherman, *Proc. Natl. Acad. Sci. USA* **2007**, *104*, 9266.
[7] K. König, *J. Microsc.* **2000**, *200*, 83.
[8] A. L. Rogach, A. Eychmüller, S. G. Hickey, S. V. Kershaw, *Small* **2007**, *3*, 536.
[9] A. M. Derfus, W. C. W. Chan, S. N. Bhatia, *Nano Lett.* **2004**, *4*, 11.
[10] X. Gao, Y. Cui, R. M. Levenson, L. W. K. Chung, S. Nie, *Nat. Biotechnol.* **2004**, *22*, 969.
[11] F. Wang, W. Tan, Y. Zhang, X. Fan, M. Wang, *Nanotechnology* **2006**, *17*, R1.
[12] J. W. Stouwdam, F. C. J. M. van Veggel, *Nano Lett.* **2002**, *2*, 733.
[13] X. Wang, J. Zhuang, Q. Peng, Y. Li, *Inorg. Chem.* **2006**, *45*, 6661.
[14] F. Wang, Y. Zhang, X. Fan, M. Wang, *J. Mater. Chem.* **2006**, *16*, 1031.
[15] S. Sivakumar, P. R. Diamente, F. C. J. M. van Veggel, *Chem. Eur. J.* **2006**, *12*, 5878.
[16] K. Kömpe, H. Borchert, J. Storz, A. Lobo, S. Adam, T. Möller, M. Haase, *Angew. Chem. Int. Ed.* **2003**, *42*, 5513.
[17] J. W. Stouwdam, F. C. J. M. van Veggel, *Langmuir* **2004**, *20*, 11763.
[18] M. M. Lezhnina, T. Jüstel, H. Kätker, D. U. Wiechert, U. H. Kynast, *Adv. Funct. Mater.* **2006**, *16*, 935.
[19] M. Lezhnina, F. Laeri, L. Benmouhadi, U. Kynast, *Adv. Mater.* **2006**, *18*, 280.
[20] J. Zhang, C. M. Shade, D. A. Chengelis, S. Petoud, *J. Am. Chem. Soc.* **2007**, *129*, 14834.
[21] S. R. Chinn, in *CRC Handbook of Laser Science and Technology, Vol. 1* (Ed.: M. J. Weber), CRC, Boca Raton, FL **1982**.
[22] C. M. Bender, J. M. Burlitch, *Chem. Mater.* **2000**, *12*, 1969.
[23] A. M. Pires, M. F. Santos, M. R. Davolos, E. B. Stucchi, *J. Alloys Compd.* **2002**, *344*, 276.
[24] D. Pi, F. Wang, X. Fan, M. Wang, Y. Zhang, *Spectrochim. Acta Part A* **2005**, *61*, 2455.
[25] O. V. Kudryavtseva, L. S. Garashina, K. K. Rivkina, B. P. Sobolev, *Sov. Phys. -Crystallogr.* **1974**, *18*, 531.
[26] J. W. Stouwdam, G. A. Hebbink, J. Huskens, F. C. J. M. van Veggel, *Chem. Mater.* **2003**, *15*, 4604.
[27] U. Kynast, M. Lezhnina, H. Kätker, *Solid State Phen.* **2005**, *106*, 93.
[28] W. Stöber, A. Fink, E. J. Bohn, *J. Colloid Interface Sci.* **1968**, *26*, 62.
[29] G. H. Dieke, in *Spectra and Energy Levels of Rare-earth Ions in Crystals*, (Eds: H. M, Crosswhite, H. Crosswhite,) Interscience, New York **1968**.
[30] W. Zhang, P. Xie, C. Duan, K. Yan, M. Yin, L. Lou, S. Xia, J. C. Krupa, *Chem. Phys. Lett.* **1998**, *292*, 133.
[31] Z. Wei, L. Sun, C. Liao, C. Yan, *Appl. Phys. Lett.* **2002**, *80*, 1447.
[32] N. O. Nuñez, M. Ocaña, *Nanotechnology* **2007**, *18*, 455606.
[33] L. Zhu, Q. Li, X. Liu, J. Li, Y. Zhang, J. Meng, X. Cao, *J. Phys. Chem. C.* **2007**, *111*, 5898.
[34] H. Deng, S. Yang, S. Xiao, H. Gong, Q. Wang, *J. Am. Chem. Soc.* **2008**, *130*, 2032.
[35] R. B. Yu, K. H. Yu, W. Wei, X. X. Xu, X. M. Qiu, S. Liu, W. Huang, G. Tang, H. Ford, B. Peng, *Adv. Mater.* **2007**, *19*, 838.
[36] R. E. Muenchausen, L. G. Jacobsohna, B. L. Bennetta, E. A. McKigneya, J. F. Smitha, J. A. Valdeza, D. W. Cookea, *J. Lumin.* **2007**, *126*, 838.
[37] V. Sudarsan, S. Sivakumar, F. C. J. M. van Veggel, *Chem. Mater.* **2005**, *17*, 4736.

ADVANCED MATERIALS

[38] G. Yi, H. Lu, S. Zhao, Y. Ge, W. Yang, D. Chen, L. Guo, *Nano Lett.* **2004**, *4*, 2191.
[39] Y. S. Lin, Y. Hung, H. Y. Lin, Y. H. Tseng, Y. F. Chen, C. Y. Mou, *Adv. Mater.* **2007**, *19*, 577.
[40] H. Ow, D. R. Larson, M. Srivastava, B. A. Baird, W. W. Webb, U. Wiesner, *Nano Lett.* **2005**, *5*, 113.
[41] D. K. Chatterjeea, A. J. Rufaihaha, Y. Zhang, *Biomaterials* **2008**, *29*, 937.